https://doi.org/10.15407/ujpe71.2.128

I. SZANYI [1, 2]

[1] HUN-REN Wigner Research Centre for Physics
(29-33, Konkoly-Thege M. Str., Budapest 1121, Hungary)
[2] MATE Institute of Technology, KRC
(36, Mátrai Str., Gyöngyös 3200, Hungary; e-mail: iszanyi@cern.ch)

STRUCTURES IN ELASTIC AND SINGLE-DIFFRACTIVE SCATTERING OF PROTONS [1]

Structures in elastic proton–proton scattering include the low-$|t|$ non-exponential behavior, as well as a diffractive minimum followed by a maximum in the $|t|$-distribution. The underlying physics of these structures and the possibility of a similar minimum–maximum pattern appearing in the $|t|$-distribution of single-diffractive scattering of protons are discussed. A simple model that describes low-mass resonances in the M^2-distribution of single-diffractive proton-proton scattering is also presented.

K e y w o r d s: elastic proton-proton scattering, diffractive scattering, single-diffractive dissociation, resonances, pomeron, odderon, "soft" processes.

1. Introduction

In high-energy proton–proton (pp) interactions, various processes may take place, including elastic scattering and single-diffractive scattering. The latter is also called single-diffractive dissociation. High-energy elastic scattering and single-diffractive processes are characterized by dominant pomeron ($\mathbb{P}$) exchange, which acts as the mediator of the strong interaction between the protons (see Fig. 1).

For elastic scattering reactions,

$$p(p_1) + p(p_2) \to p(p_1') + p(p_2'),$$

the independent kinematic variables are the squared center of mass energy, $s = (p_1 + p_2)^2$, and the squared four-momentum transfer, $t = (p_1 - p_1')^2$, where p_i ($i \in \{1, 2\}$) are the initial-state four-momenta, and p_i' are the final-state four-momenta of the protons.

Single diffractive dissociation of protons is a process

$$p(p_1) + p(p_2) \to p(p_1') + X(p_X),$$

where X denotes all the particles that may be produced together with an intact proton in the final state. In this case, the independent kinematic variables are: $s = (p_1 + p_2)^2$, $t = (p_1 - p_1')^2$, and $M^2 = (p_1 + p_2 - p_1')^2$, the squared mass of the produced hadronic system X.

In this paper, we focus on "soft" scattering processes. In the "soft" domain, the perturbative methods of quantum chromodynamics (QCD), the fundamental theory of strong interactions, are not applicable due to the large value of the strong coupling. Comprehensive theoretical investigations of the existing experimental data can be carried out by relying on S-matrix theory, optical analogies, and Regge theory [1].

Structures in elastic proton–proton scattering include the low-$|t|$ non-exponential behavior and the characteristic minimum-maximum structure of the t-distribution. These structures were first observed at the ISR accelerator at CERN in the 1970s [2, 3] in the energy range of 23 GeV $\lesssim \sqrt{s} \lesssim$ 63 GeV and later confirmed at LHC by the TOTEM experiment [4–9] in the energy range of 2.76 GeV $\leq \sqrt{s} \leq$ $\leq$ 13 TeV. At $\sqrt{s} = 8$ TeV, the TOTEM results exclude a purely exponential shape, $Ae^{-B|t|}$, in the range of 0.027 GeV$^2 \lesssim |t| \lesssim$ 0.2 GeV^2 with a significance greater than 7σ [5].

Regarding structures in dissociation processes, nucleon and baryon resonances were seen at low

Citation: Szanyi I. Structures in elastic and single-diffractive scattering of protons. *Ukr. J. Phys.* **71**, No. 2, 128 (2026). https://doi.org/10.15407/ujpe71.2.128.

[1] This work is based on the results presented at the 2025 "New Trends in High-Energy Physics" Conference.

masses in the M^2-distribution of inclusive dissociation processes [10–13] in pp and proton-deuteron (pd) collisions. Similar resonance structures are expected at LHC energies [14] in single-diffractive dissociation of protons. Another expected structure in the single-diffractive dissociation of protons is a minimum–maximum pattern in the $|t|$-distribution, see Ref. [15]. However, such a structure has not yet been observed in the measured data, possibly due to the limited $|t|$-acceptance of the experiments.

This paper is organized as follows. In Sec. 2, after introducing the basic formalism for elastic hadronic scattering, the structures in the t-distribution of elastic pp (and proton-antiproton, $p\bar{p}$) scattering are discussed. In Sec. 3, the formalism for inclusive hadronic dissociation is introduced, and then structures in the t- and M^2-distribution of single-diffractive dissociation of protons are investigated. A short summary is given in Sec. 4.

2. Elastic Scattering of Protons

2.1. Elastic hadronic scattering formalism

There are two basic approaches for treating "soft" elastic reactions [16]: the s-channel formalism and the t-channel formalism.

In the s-channel formalism, elastic scattering is related to the particle formation in the direct channel: the incident proton wave is partly absorbed due to many open inelastic interaction channels at high energies; this leads to diffraction, and the diffracted waves add up coherently giving rise to a sharp forward peak in the t-distribution [17–19], called the diffraction cone. The schematic representation of high-energy particle diffraction is presented in Fig. 2.

The formulas that describe high-energy, "soft" scattering of particles are analogous to those describing Fraunhofer diffraction of light by absorbing obstacles [16]. The characteristics of the "obstacle" at a given s and impact parameter b are specified by the complex profile function, $\Gamma(s,b)$. The elastic scattering amplitude, $A_{\rm el}(s,t)$, is related to the Fourier transform of the profile function:

$$A_{\rm el}(s,t) = \frac{is}{2\pi}\int d^2\mathbf{b}e^{i\mathbf{q}\cdot\mathbf{b}}\Gamma(s,b), \qquad (1)$$

where $q = |\mathbf{q}| \equiv \sqrt{-t}$ with $\mathbf{q}$ being the two-dimensional transverse momentum transfer vector in the reaction, and $b = |\mathbf{b}|$ with $\mathbf{b}$ being the two-dimensional impact parameter vector in the transverse plane.

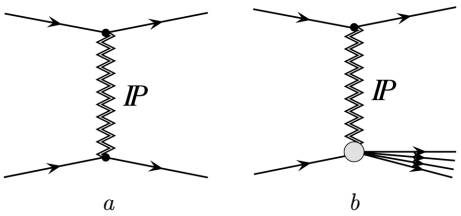

Fig. 1. Elastic (a) and single-diffractive (b) scattering with lowest order pomeron exchange

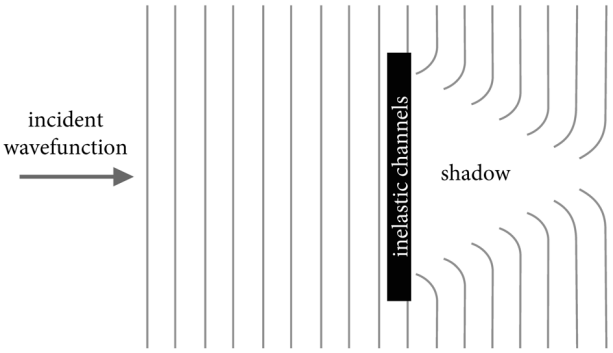

Fig. 2. Schematic representation of high-energy particle diffraction

The experimentally measurable differential cross-section of elastic scattering is:

$$\frac{{\rm d}\sigma_{\rm el}}{{\rm d}t}(s,t) = \frac{\pi}{s^2}\left|A_{\rm el}\left(s,t\right)\right|^2. \qquad (2)$$

In the t-channel approach to elastic scattering, the scattering amplitude is given in terms of t-channel (virtual) exchange contributions. In this paper, the focus is on the t-channel approach.

In the framework of T. Regge's theory of complex angular momenta, the high-energy behavior of the relativistic scattering amplitude is determined by the singularities of the partial wave amplitudes in the complex angular momentum plane [16].

The t-channel scattering amplitude of signature $\xi = \pm 1$ is:

$$A^{\xi}_{\rm el}(s,t) = 2i\int\limits_C (2j+1)\, f^{\xi}(j,t)\,\frac{P_j(-z_t)}{\sin(\pi j)}\,dj, \qquad (3)$$

where $f^{\xi}(j,t)$ is the partial wave amplitude of signature ξ and complex angular momentum j, P_j is the Legendre polynomial of degree j, and

$$z_t = 1 + \frac{2s}{t-4m_p},$$

with m_p being the mass of the proton.

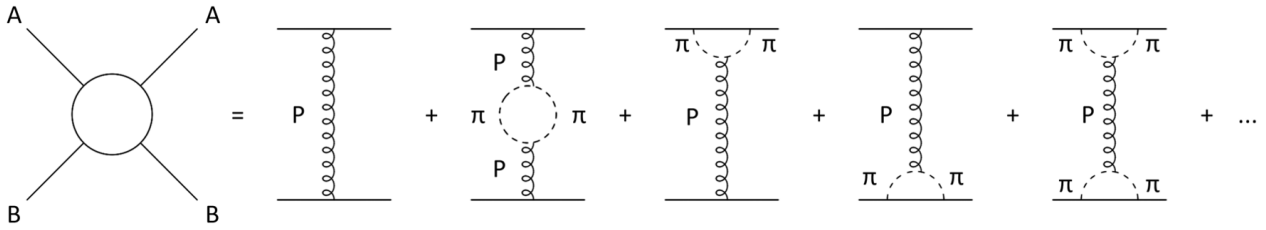

Fig. 3. Schematic diagram for elastic scattering with two-pion production contributions

If the singularity is a simple pole,

$$f(j,t) \underset{j\to\alpha(t)}{\sim} \frac{\beta(t)}{j-\alpha(t)}, \tag{4}$$

we have a Regge trajectory, $\alpha^{\xi}(t)$ exchange or reggeon exchange with signature ξ. A reggeon exchange can be interpreted as an exchange of a virtual particle with continuously varying spin ($j = \mathrm{Re}\,\alpha^{\xi}(t)$) and virtuality ($Q^2 = -t$).

At high energies, the dominant contribution comes from the pomeron exchange. The contribution of a simple-pole pomeron ($\xi = +1$) is

$$A^{\mathbb{P}}_{\mathrm{el}}(s,t) = g^2_{\mathbb{P}pp}(t)\frac{-e^{-i\pi\alpha_{\mathbb{P}}(t)/2}}{\sin(\pi\alpha_{\mathbb{P}}(t)/2)}\left(\frac{s}{s_0}\right)^{\alpha_{\mathbb{P}}(t)}, \tag{5}$$

where $g_{\mathbb{P}pp}(t)$ is the Pomeron-proton coupling [2].

It is usual to absorb the

$$\frac{1}{\sin(\pi\alpha_{\mathbb{P}}(t)/2)}$$

factor into the coupling and write that

$$A^{\mathbb{P}}_{\mathrm{el}}(s,t) = -e^{-i\pi\alpha_{\mathbb{P}}(t)/2}g^2_{\mathbb{P}pp}(t)\left(\frac{s}{s_0}\right)^{\alpha_{\mathbb{P}}(t)}, \tag{6}$$

where typically $s_0 = 1$ GeV^2.

This simple pole pomeron exchange picture with an exponential Pomeron-proton coupling,

$$g^2_{\mathbb{P}pp}(t) = e^{b_{\mathbb{P}}t},$$

and a real-valued linear Regge trajectory,

$$\alpha_{\mathbb{P}}(t) = 1 + \delta_{\mathbb{P}} + \alpha'_{\mathbb{P}}t,$$

with $\delta_{\mathbb{P}} \simeq 0.08$ and $\alpha'_{\mathbb{P}} \simeq 0.25$ GeV^{-2}, reproduces the main features of the high-energy pp and $p\bar{p}$ elastic scattering. These features are, see Ref. [21]: (i) the rise of the total cross section,

$$\sigma_{\mathrm{tot}}(s) = \frac{4\pi}{s}\,\mathrm{Im}\,A_{\mathrm{el}}(s,t=0), \tag{7}$$

with increasing s, (ii) the forward peak in the elastic differential cross section, and (iii) the energy evolution of its slope (shrinkage of the diffraction cone). Note, however, a subdominant exchange with negative signature, $\xi = -1$ (the odderon), higher-order poles (multiple poles), cut singularities, and non-linear complex trajectories are also possible and important both theoretically and phenomenologically, as they account for the finer details observed in the experimental data [1, 16, 21–26].

The phenomenological importance of non-linear complex Regge trajectories, the double-pole exchanges, and the odderon exchange is discussed below.

2.2. Low-t non-exponential behavior

In the t-channel Regge exchange picture of elastic scattering, the non-exponential low-$|t|$ differential cross section is related to the two-pion production threshold ($4m_\pi^2$) branch point of the t-channel scattering amplitude and, hence, is explained as the manifestation of t-channel unitarity, see Refs. [27–33]. In Ref. [33], it was discussed that the non-exponential behavior of the low-$|t|$ $d\sigma_{\mathrm{el}}/dt$ can come from both the non-linear pomeron trajectory and the non-linear pomeron-proton vertex coupling (a schematic representation is presented in Fig. 3). In this case, both the pomeron trajectory and the pomeron-proton vertex coupling factor become complex and non-linear:

$$\alpha_{\mathbb{P}}(t) = \alpha_{\mathbb{P}0} + \alpha'_{\mathbb{P}}t - \alpha_{1P}\left(\sqrt{4m_\pi^2 - t} - 2m_\pi\right), \tag{8}$$

$$g_{\mathbb{P}pp}(t) = e^{b_{\mathbb{P}}t + \beta_{\mathbb{P}}\left(\sqrt{4m_\pi^2 - t} - 2m_\pi\right)}. \tag{9}$$

A model implementing these ideas successfully describes the non-exponential behavior of the data from ISR to LHC energies [33] as presented in Fig. 4.

[2] Due to unitarity, for a simple pole, residues of the poles factorize [20].

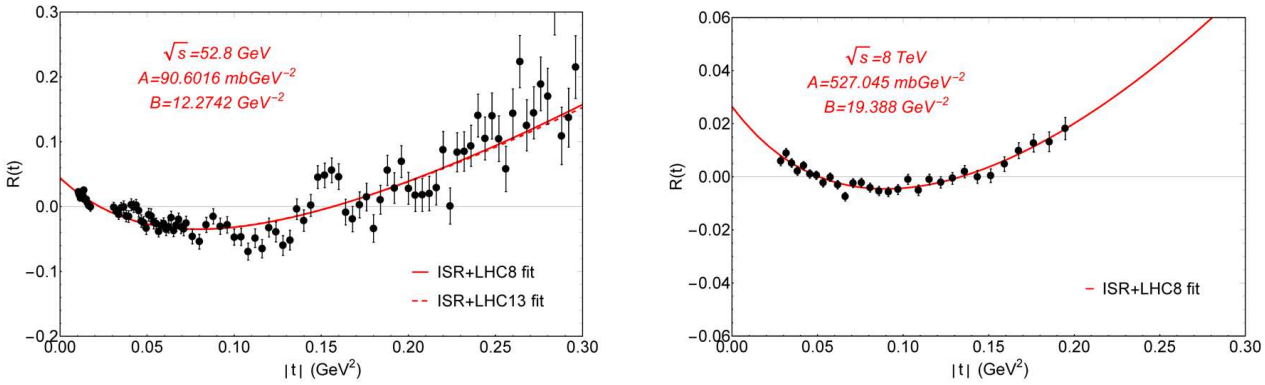

Fig. 4. Differential cross section for pp scattering at $\sqrt{s} = 52.8$ GeV and $\sqrt{s} = 8$ TeV compared to reference exponentials: $R(t) = 1 - \frac{d\sigma_{\rm el}/dt}{\rm ref(t)}$ with $\rm ref(t) = Ae^{Bt}$ fitted to the data

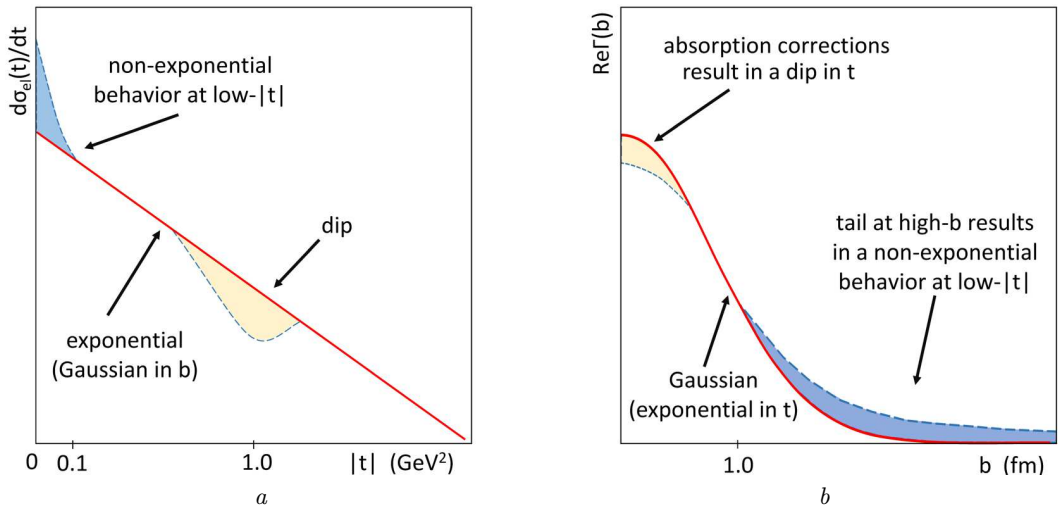

Fig. 5. Schematic connection between (a) the t-dependence (differential cross section) and (b) the b-dependence (profile function) of elastic pp scattering

In the s-channel picture of elastic scattering, the strong non-exponential behavior at low-$|t|$ in the differential cross section can be reproduced by a $\Gamma(s,b)$ profile function that has a power law tail at high-b values. Note that the dominant pomeron exchange amplitude is dominantly imaginary, and hence, via Eq. (1), $\Gamma(s,b)$ is predominantly real. A schematic connection between the t-dependence and b-dependence of elastic scattering is presented in Fig. 5. A profile function with a Lévy α-stable shape in b and $\alpha_L < 2$ successfully describes the measured data, see Refs. [34, 35].

The authors of Refs. [36, 37] argue that the low-$|t|$ non-exponential behavior of the elastic pp differential cross section can be a consequence of an interplay between the real parts of the Coulomb and nuclear amplitudes. Further quantitative investigation of the interplay between the two-pion production contribution and the Coulomb effects is a subject for future studies.

2.3. Minimum-maximum structure

The minimum-maximum structure in pp scattering is related to s-channel unitarity, that is, absorption corrections: a reduction at small-b in the $\Gamma(s,b)$ profile function (see Fig. 5). This reduction physically corresponds to absorption of the incoming particle flux into channels other than those studied, see Ref. [38]. Ab-

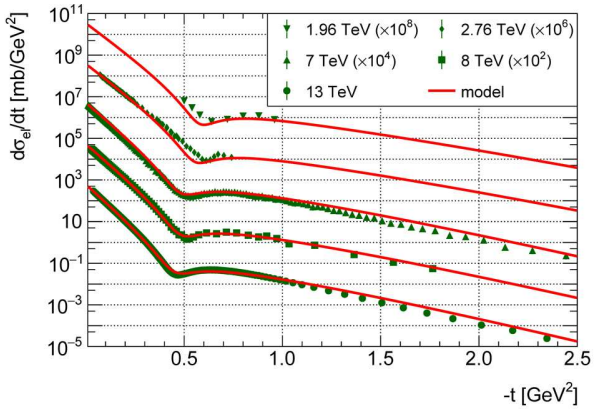

Fig. 6. Elastic pp differential cross section data described by a dipole Regge exchange model with both pomeron and odderon contributions

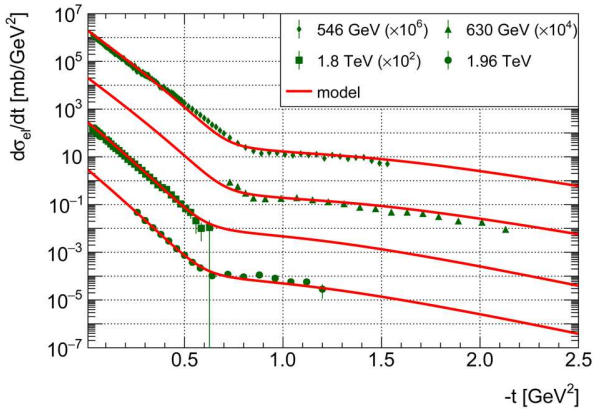

Fig. 7. Elastic $p\bar{p}$ differential cross section data described by a dipole Regge exchange model with both pomeron and odderon contributions

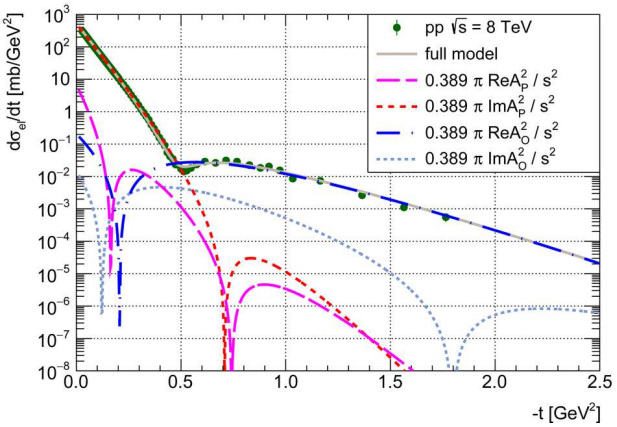

Fig. 8. Contribution of the real and imaginary parts of the pomeron and odderon components of the amplitude to the description of the pp differential cross section data at $\sqrt{s} = 8$ TeV

sorption corrections (or s-channel unitarity corrections) are accounted for by the contribution of multiple or multipole Reggeon exchanges.

The dipole pomeron exchange model is a simple model for describing the minimum-maximum structure in elastic pp scattering as a result of absorption corrections. This was developed in the 1970s by Prof. L. Jenkovszky and his coauthors [39, 40].

In the dipole Regge exchange model, the high-energy behavior of the elastic scattering amplitude is determined by an isolated j-plane second-order pole (dipole) of the partial wave amplitude [41],

$$f(j,t) = \frac{\beta(j)}{[j-\alpha(t)]^2}, \tag{10}$$

where the residue $\beta(j)$ is t-independent and non-singular at $j = \alpha(t)$; $\alpha(t)$ is the Regge trajectory.

The first version of a dipole odderon amplitude was introduced in the 1980s, see Ref. [42]. The model that included dipole pomeron and odderon amplitude components was used to analyze pp and $p\bar{p}$ elastic scattering data below LHC energies in a number of papers, see Refs. [42–44]. Later this dipole model was used also to analyze LHC measurements, see Refs. [45–48]. This rather simple model with dipole pomeron and odderon components is sometimes referred to as the Jenkovszky model.

Recently, this dipole Regge exchange model with both pomeron and odderon contributions was applied in Ref. [15] to describe pp and $p\bar{p}$ elastic scattering differential cross section data from SPS energies ($\sqrt{s} \simeq 500$ GeV) up to LHC energies. The results are presented in Fig. 6 and Fig. 7. Fig. 8 demonstrates that the inclusion of the dipole odderon is important for describing the data around the dip-bump and at higher $|t|$ values.

3. Single Diffraction Dissociation

3.1. Formalism for proton dissociation

By combining the Regge exchange model for single proton dissociation with Mueller's generalized optical theorem, we obtain the following expression for the high-energy double differential cross section of the process, see Ref. [38]:

$$\frac{d^2\sigma_{SD}}{dtdM^2} = \frac{1}{16\pi^2 s^2} \sum_{ijk} \Big[g_{ipp}(t) g^*_{jpp}(t) \eta_i(t) \eta^*_j(t) \times$$

$$\times \left(\frac{s}{M^2}\right)^{\alpha_i(t)} \left(\frac{s}{M^2}\right)^{\alpha_j(t)} \frac{M^2}{s_0}\sigma^{\rm tot}_{ijk}(M^2,t)\Bigg], \qquad (11)$$

where $g_i(t)$ is the coupling between reggeon i and the proton;

$$\eta_i(t) = \frac{\xi + e^{-i\pi\alpha_i(t)}}{\sin(\pi\alpha_i(t))},$$

is the signature factor of reggeon i and $\xi = \pm 1$ is its signature; $\left(\frac{s}{M^2}\right)^{\alpha_i(t)}$ is the propagator factor of reggeon i obtained by assuming that $s \gg M^2 \gg \gg t \gg m_p^2$; $\sigma^{\rm tot}_{i,j,k}(M^2,t)$ is the total cross section for reggeon proton scattering with incoming reggeon i, outgoing reggeon j via a mediator reggeon k at an "energy", M^2, and with ingoing/outgoing reggeon "mass-squared" (virtuality), t; the factor M^2/s_0 just before $\sigma^{\rm tot}_{ijk}(M^2,t)$ is the inverse of the flux factor which is inserted in order to write cross section instead of ${\rm Im}A_{ip\to jp}(t,M^2,\tilde{t}=0)$, the reggeon particle scattering amplitude at $\tilde{t}=0$. For high masses, *i.e.*, $M^2 \to \infty$:

$$\sigma^{\rm tot}_{ijk}(M^2,t) = \frac{1}{M^2/s_0}{\rm Im}A_{ip\to jp}(t,M^2,\tilde{t}=0) \equiv$$
$$\equiv \frac{1}{s_0} g_{kpp}(0) g_{ijk}(t,0) \left(\frac{M^2}{s_0}\right)^{\alpha_k(0)-1}, \qquad (12)$$

where $g_{kpp}(0)$ is the reggeon-proton coupling k at $\tilde{t} = 0$, and $g_{ijk}(t,0)$ is the triple-reggeon coupling between reggeons i, j, and k at $\tilde{t}=0$; we set $s_0 = 1$ GeV^2.

3.2. Low-mass resonances

Let us assume that we have diffractive dissociation, and the $pp \to pX$ process occurs via pomeron exchange alone. Then Eq. (11) takes the form

$$\frac{d^2\sigma_{SD}}{dtdM^2} = \frac{1}{16\pi^2 s^2} \times$$
$$\times \left[g^2_{\mathbb{P}pp}(t) \left(\frac{s}{M^2}\right)^{2\alpha_{\mathbb{P}}(t)} \frac{M^2}{s_0}\sigma^{\rm tot}_{\rm PPP}(M^2,t)\right], \qquad (13)$$

where, for simplicity, we set

$$g^2_{\mathbb{P}pp}(t) = ae^{bt}.$$

For the pomeron $\xi = 1$ and the remainder of the signature factor, $1/\sin(\pi\alpha_{\mathbb{P}}(t)/2)$, is absorbed into $g^2_{\mathbb{P}pp}(t)$; this can be done since $g_{\mathbb{P}pp}(t)$ is not fixed by Regge theory itself and one has to model its t-dependence. We use a simple linear pomeron trajectory:

$$\alpha_{\mathbb{P}}(t) = 1 + \delta_{\mathbb{P}} + \alpha'_{\mathbb{P}} t,$$

where the typical values are, see Ref. [49]: $\delta_{\mathbb{P}} = 0.08$ and $\alpha'_{\mathbb{P}} = 0.25$ GeV^{-2}.

Now we want to make $\sigma^{\rm tot}_{\rm PPP}(M^2,t)$ valid at low-M^2 and not only in the asymptotic, $M^2 \to \infty$ region. We rewrite it as a sum of three different components:

$$\sigma^{\rm tot}_{\rm PPP}(M^2,t) = \sigma^{\rm tot,\,asy}_{PPP}(M^2,t) +$$
$$+ \sigma^{\rm tot,\,Rop}_{\rm PPP}(M^2,t) + \sigma^{\rm tot,\,N}_{\rm PPP}(M^2,t), \qquad (14)$$

where

$$\sigma^{\rm tot,\,asy}_{PPP}(M^2,t) = \left(1 - \frac{M^2_{\rm th}}{M^2}\right) \times$$
$$\times \frac{c_{\rm asy}}{\sqrt{\lambda(M^2,t,m_p^2)}} \left(\frac{M^2}{s_0}\right)^{\alpha_{\mathbb{P}}(0)} \qquad (15)$$

is the Regge asymptotic component that describes the high-M^2 domain and also serves as a background in the low-M^2 region ($\lambda(x,y,z)$ is the usual Källén function and the threshold mass for proton dissociation is $M_{\rm th} = m_p + m_{\pi^0}$); $\sigma^{\rm tot,\,Rop}_{PPP}(M^2,t)$ describes the contribution of the Roper resonance; and $\sigma^{\rm tot,\,N}_{PPP}(M^2,t)$ describes the contribution of the nucleon resonances.

The Roper-resonance term is parametrized by a Breit–Wigner function:

$$\sigma^{\rm tot,\,Rop}_{\rm PPP}(M^2,t) = \left(1 - \frac{M^2_{\rm th}}{M^2}\right) \frac{c_{\rm Rop} e^{b_{\rm Rop}t}}{\sqrt{\lambda(M^2,t,m_p^2)}} \times$$
$$\times \frac{M_{\rm Rop}\Gamma_{\rm Rop}}{\left(M^2 - M^2_{\rm Rop}\right)^2 - M^2_{\rm Rop}\Gamma^2_{\rm Rop}}, \qquad (16)$$

where $M_{\rm Rop} = 1.44$ GeV and $\Gamma_{\rm Rop} = 0.325$ GeV. An exponential factor is included to introduce a t-dependence for the Roper-resonance contribution that provides a good description of the data.

The contribution of the nucleon resonances is constructed based on the pole decomposition of dual amplitudes with Mandelstam analyticity (DAMA) [14, 50]:

$$\sigma^{\rm tot,\,N}_{PPP}(M^2,t) = \left(1 - \frac{M^2_{\rm th}}{M^2}\right) \frac{c_{\rm N}}{\sqrt{\lambda(M^2,t,m_p^2)}} \times$$
$$\times \sum_J \frac{{\rm Im}\alpha_{N^*}(M^2)}{(J - {\rm Re}\alpha_{N^*}(M^2))^2 + ({\rm Im}\,\alpha_{N^*}(M^2))^2}, \qquad (17)$$

where α_{N^*} is the complex, non-linear nucleon trajectory [51] with parameters given in Ref. [14]. DAMA

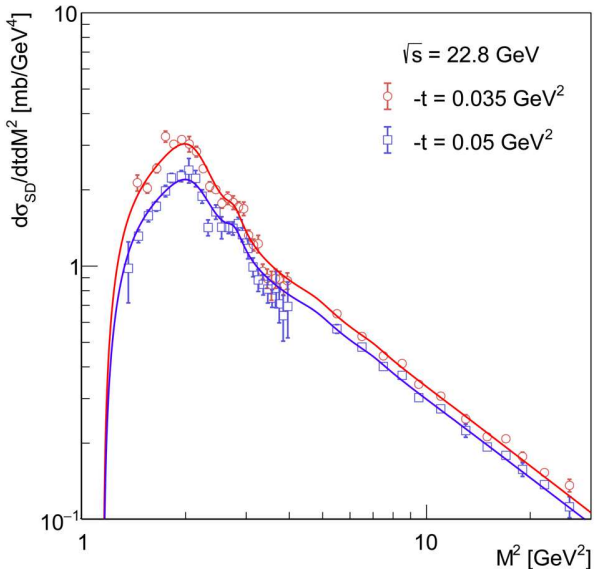

Fig. 9. M^2-dependence at $-t = 0.035$ GeV^2 and $-t = 0.05$ GeV^2 from low-M^2 resonance region up to the asymptotic, higher-M^2 values

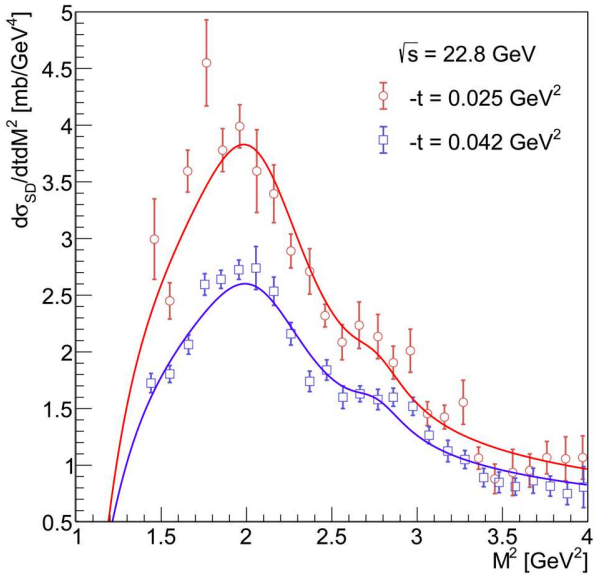

Fig. 10. M^2-dependence at $-t = 0.025$ GeV^2 and $-t = 0.042$ GeV^2 in the low-M^2 resonance region

not only allows for but also requires complex, nonlinear Regge trajectories.

The described model has six free parameters a, b, c_{asy}, b_{Rop}, c_{Rop}, c_{N}. These are fitted [3] to pd (proton-deuteron) inclusive scattering proton dissociation ($pd \to Xd$) data transformed into pp (proton-proton) inclusive scattering proton dissociation ($pp \to Xp$) data using the $F_d(t)$ coherence factor, see Refs. [10, 11]. A study is performed using data at a center-of-mass energy of $\sqrt{s} = 22.8$ GeV, which corresponds to a proton laboratory momentum of $p_L = 275$ GeV in the original fixed-target experiment. The values of the fitted parameters and the fit statistics are given in Table. The results are graphically presented in Figs. 9 and 10. Fig. 11 shows the contributions from the resonances and the asymptotic component separately.

[3] The model is fitted to the data by including the conversion factor 0.3894 (in natural units 1 GeV^{-2} = 0.3894 mb).

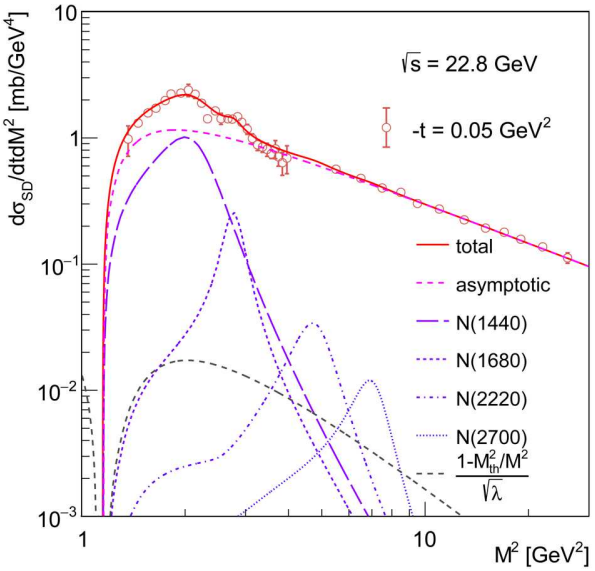

Fig. 11. M^2-dependence at $-t = 0.05$ GeV^2. The contributions from the resonances and the asymptotic component are shown separately

Parameter values for the resonance model

Parameter	Value
a	60.3 ± 2.6
b [GeV^{-2}]	5.5 ± 0.5
c_{asy}	13.3 ± 0.6
b_{Rop} [GeV^{-2}]	22.4 ± 2.1
c_{Rop} [GeV^2]	36.6 ± 3.0
c_{N}	2.6 ± 0.3
χ^2	242.2
NDF	123
χ^2/NDF	1.97

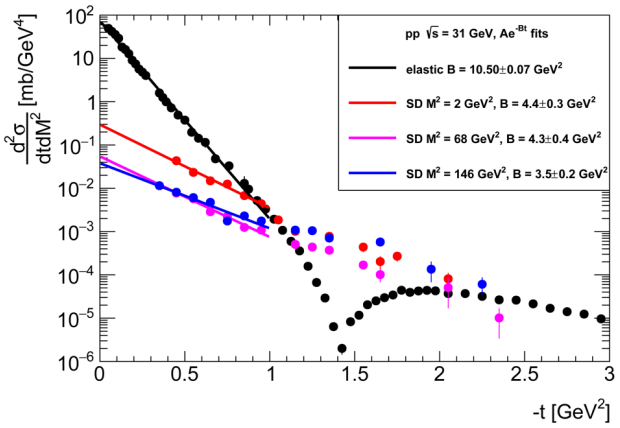

Fig. 12. Elastic pp scattering and single-diffractive dissociation differential cross section data at $\sqrt{s} = 31$ GeV as a function of $-t$

These results provide a solid basis for a more complete analysis of all the existing inclusive proton dissociation data in the future. Once this analysis is completed, it will allow for more precise predictions for the proton dissociation cross section in pp scattering at LHC energies in the low-M^2 domain.

3.3. Minimum-maximum structure

Measurements of pp single diffractive dissociation at ISR do not show a dip-bump structure at $|t|$ values where such a structure is observed in elastic pp scattering. This is illustrated in Fig. 12 based on the single diffractive dissociation data from Ref. [52]. This observation can be explained in the framework of a dipole Regge model in which the dip-bump structure moves to higher $|t|$ values as the value of the slope parameter decreases, see Ref. [15].

In Ref. [15] a dipole pomeron + odderon Regge approach was utilized to predict dip-bump structures in pp single diffractive dissociation at LHC energies. The starting point of the model is the triple-reggeon approach for single diffraction. The full double differential cross section has four components:

$$\frac{d^2\sigma_{SD}}{dtdM^2}(s,t,M^2) = \frac{d^2\sigma_{SD}^{\rm PPP}}{dtdM^2} + \frac{d^2\sigma_{SD}^{\rm OOP}}{dtdM^2} + \\ + \frac{d^2\sigma_{SD}^{\rm RRP}}{dtdM^2} + \frac{d^2\sigma_{SD}^{\pi}}{dtdM^2}, \qquad (18)$$

where $d^2\sigma_{SD}^{\rm PPP}/dtdM^2$ is the dipole pomeron-pomeron-pomeron vertex contribution, $d^2\sigma_{SD}^{\rm OOP}/dtdM^2$ is the dipole odderon-odderon-pomeron vertex contribution, $d^2\sigma_{SD}^{\rm RRP}/dtdM^2$ is an effective reggeon-reggeon-pomeron contribution, and $d^2\sigma_{SD}^{\pi}/dtdM^2$ is a pion exchange contribution. The main results are presented in Figs. 13 and 14, showing the different cross section components separately. The main conclusion are: (i) a dip-bump structure is predicted around $t = -4.5$ GeV^2 at LHC and SPS energies in the range of 3 GeV$^2 \lesssim |t| \lesssim 7$ GeV^2; (ii) the position of the dip and bump in $-t$ in single diffractive dissociation changes slowly with M and is determined by the dipole OOP contribution.

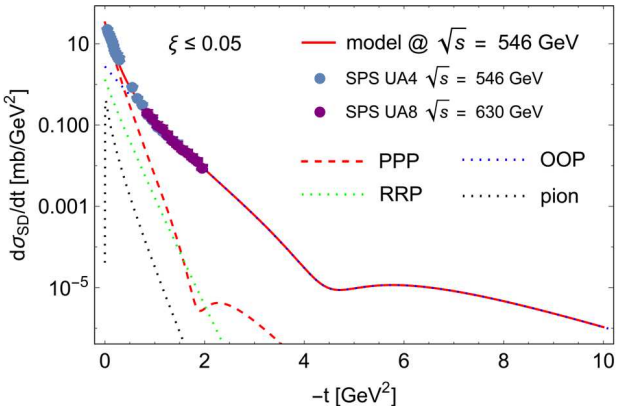

Fig. 13. Prediction to a minimum-maximum structure in proton's single diffraction at SPS energy $\sqrt{s} = 546$ GeV

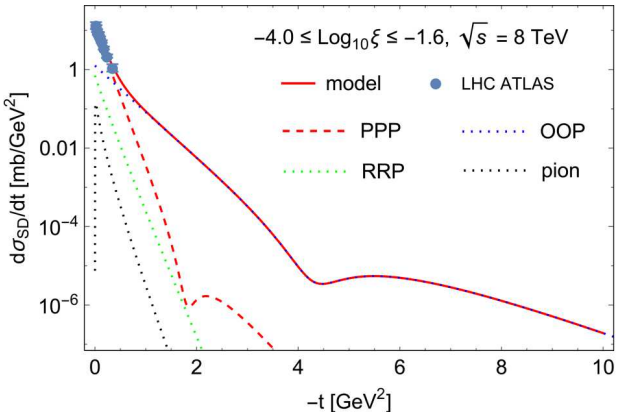

Fig. 14. Prediction to a minimum-maximum structure in proton's single diffraction at LHC energy $\sqrt{s} = 8$ TeV

4. Summary

Structures in elastic and single diffractive pp scattering are reviewed.

The low-$|t|$ non-exponential behavior of the pp elastic differential cross section is a manifestation of t-

channel unitarity: the data can be described from ISR energies up to LHC energies by considering the contribution of the branch point of the t-channel scattering amplitude at the two-pion production threshold.

The minimum–maximum structure is connected to s-channel unitarity: absorption corrections, accounted for by multipole Reggeon exchanges, reduce the profile function $\Gamma(s,b)$ at small-b and generate a dip in the $|t|$-distribution.

A minimum–maximum structure is expected in the $|t|$-distribution of single diffractive pp scattering around $t = -4.5$ GeV^2 at LHC and SPS energies in the range of 3 GeV$^2 \lesssim |t| \lesssim 7$ GeV^2 based on a model containing a dipole pomeron and odderon contributions.

A simple model is constructed and fitted to the data on single diffractive scattering in the low-M^2 resonance region. The dominant resonances at $\sqrt{s} = 22.8$ GeV, before the asymptotic M^2-behavior sets in, are the N(1440) Roper resonance, N(1680), and N(2220).

The author is grateful to the late Prof. L. Jenkovszky for introducing him to the field of high-energy physics, and for his mentorship and profound ideas that significantly contributed to the completion of the presented work. The author also thanks R. Schicker for the fruitful discussions.

The author's work was supported by the Research Excellence Programme of MATE, the Hungarian University of Agriculture and Life Sciences.

1. L.L. Jenkovszky. High-energy elastic hadron scattering. *Riv. Nuovo Cim.* **10** (12), 1 (1987).
2. G. Barbiellini *et al.* Small angle proton proton elastic scattering at very high-energies ($460 < s < 2900$ GeV^2). *Phys. Lett. B* **39**, 663 (1972).
3. E. Nagy *et al.* Measurements of elastic proton proton scattering at large momentum transfer at the CERN intersecting storage rings. *Nucl. Phys. B* **150**, 221 (1979).
4. G. Antchev *et al.* (TOTEM). Measurement of proton-proton elastic scattering and total cross-section at $\sqrt{s} =$ $= 7$ TeV. *Europhys. Lett.* **101**, 21002 (2013).
5. G. Antchev *et al.* (TOTEM). Evidence for non-exponential elastic proton–proton differential cross-section at low $|t|$ and $\sqrt{s} = 8$ TeV by TOTEM. *Nucl. Phys. B* **899**, 527 (2015).
6. G. Antchev *et al.* (TOTEM). First determination of the ρ parameter at $\sqrt{s} = 13$ TeV: probing the existence of a colourless C-odd three-gluon compound state. *Eur. Phys. J. C* **79**, 785 (2019).
7. G. Antchev *et al.* (TOTEM). Elastic differential cross-section measurement at $\sqrt{s} = 13$ TeV by TOTEM. *Eur. Phys. J. C* **79**, 861 (2019).
8. G. Antchev *et al.* (TOTEM). Elastic differential cross-section $\mathrm{d}\sigma/\mathrm{d}t$ at $\sqrt{s} = 2.76$ TeV and implications on the existence of a colourless C-odd three-gluon compound state. *Eur. Phys. J. C* **80**, 91 (2020).
9. G. Antchev *et al.* (TOTEM). Characterisation of the dip-bump structure observed in proton–proton elastic scattering at $\sqrt{s} = 8$ TeV. *Eur. Phys. J. C* **82**, 263 (2022).
10. Y. Akimov *et al.* Excitation of high-energy protons into low mass states in $p - d$ interactions. *Phys. Rev. Lett.* **35**, 763 (1975).
11. Y. Akimov *et al.* Diffraction dissociation of high-energy protons in $p - d$ interactions. *Phys. Rev. Lett.* **35**, 766 (1975).
12. V. Bartenev *et al.* Proton proton diffraction dissociation at incident energies from 175 GeV to 400 GeV. *Phys. Lett. B* **51**, 299 (1974).
13. R.M. Edelstein *et al.* Isobar production and elastic scattering in $p - p$ interactions from 6 GeV/c to 30 GeV/c. *Phys. Rev. D* **5**, 1073 (1972).
14. L.L. Jenkovszky, O.E. Kuprash, J.W. Lamsa, V.K. Magas, R. Orava. Dual-regge approach to high-energy, low-mass diffraction dissociation. *Phys. Rev. D* **83**, 056014 (2011).
15. L. Jenkovszky, R. Schicker, I. Szanyi. Dip-bump structure in proton's single diffractive dissociation at the Large Hadron Collider. *Universe* **10**, 208 (2024).
16. V. Barone, E. Predazzi. *High-Energy Particle Diffraction* (Springer-Verlag, 2002), Vol. 565 [ISBN: 978-3-540-42107-8].
17. M.L. Good, W.D. Walker. Diffraction disssociation of beam particles. *Phys. Rev.* **120**, 1857 (1960).
18. E. Feinberg, I. Pomerančuk. High energy inelastic diffraction phenomena. *Nuovo Cim.* **3** (Suppl. 4), 652 (1956).
19. A.B. Kaidalov. Diffractive production mechanisms. *Phys. Rept.* **50**, 157 (1979).
20. V.N. Gribov. The theory of complex angular momenta: Gribov lectures on theoretical physics. In: *Cambridge Monographs on Mathematical Physics* (Cambridge University Press, 2007) [ISBN: 978-0-521-03703-7, 978-0-521-81834-6, 978-0-511-05504-1].
21. G. Matthiae. Proton and anti-proton cross-sections at high-energies. *Rept. Prog. Phys.* **57**, 743 (1994).
22. T. Csörgő, T. Novák, R. Pasechnik, A. Ster, I. Szanyi. Evidence of Odderon-exchange from scaling properties of elastic scattering at TeV energies. *Eur. Phys. J. C* **81**, 180 (2021).
23. T. Csörgő, I. Szanyi. Observation of Odderon effects at LHC energies: A real extended Bialas–Bzdak model study. *Eur. Phys. J. C* **81**, 611 (2021).
24. T. Csörgő, T. Novák, R. Pasechnik, A. Ster, I. Szanyi. Proton holography discovering odderon from scaling properties of elastic scattering. *EPJ Web Conf.* **235**, 06002 (2020).

25. V.M. Abazov *et al.* (D0, TOTEM). Odderon exchange from elastic scattering differences between pp and $p\bar{p}$ Data at 1.96 TeV and from pp forward scattering measurements. *Phys. Rev. Lett.* **127**, 062003 (2021).
26. I. Szanyi. Odderon exchange in elastic proton-proton and proton-antiproton scattering at TeV energies. *Ph.D. thesis Eotvos U.* (2024). arXiv: 2505.22790 [hep-ph].
27. G. Cohen-Tannoudji, V.V. Ilyin, L.L. Jenkovszky. A model for the pomeron trajectory. *Lett. Nuovo Cim.* **5** (S2), 957 (1972).
28. A.A. Anselm, V.N. Gribov. Zero pion mass limit in interactions at very high-energies. *Phys. Lett. B* **40**, 487 (1972).
29. C.-I. Tan, D.M. Tow. Can pions be the dominant linkage in multiperipheral cluster models? *Phys. Lett. B* **53**, 452 (1975).
30. V.A. Khoze, A.D. Martin, M.G. Ryskin. Soft diffraction and the elastic slope at Tevatron and LHC energies: A MultiPomeron approach. *Eur. Phys. J. C* **18**, 167 (2000).
31. L. Jenkovszky, A. Lengyel. Low-$|t|$ structures in elastic scattering at the LHC. *Acta Phys. Polon. B* **46**, 863 (2015).
32. D.A. Fagundes, L. Jenkovszky, E.Q. Miranda, G. Pancheri, P.V.R.G. Silva. Fine structure of the diffraction cone: from ISR to the LHC. In: *Gribov-85 Memorial Workshop on Theoretical Physics of XXI Century, 2015* (World Scientific, 2016). Pp. 180–194. arXiv: 1509.02197 [hep-ph].
33. L. Jenkovszky, I. Szanyi, C.-I. Tan. Shape of proton and the pion cloud. *Eur. Phys. J. A* **54**, 116 (2018).
34. T. Csörgő, S. Hegyi, I. Szanyi. Simple Lévy α-stable model analysis of elastic pp and $p\bar{p}$ low-$|t|$ data from SPS to LHC energies. *Universe* **10**, 127 (2024).
35. T. Csörgő, S. Hegyi, I. Szanyi. Lévy α-stable model for the non-exponential low-$|t|$ proton–proton differential cross-section. *Universe* **9**, 361 (2023).
36. A.K. Kohara. Forward scattering amplitudes of pp and $p\bar{p}$ with crossing symmetry and scaling properties. *J. Phys. G* **46**, 125001 (2019).
37. A.K. Kohara, E. Ferreira, M. Rangel. The interplay of hadronic amplitudes and Coulomb phase in LHC measurements at 13 TeV. *Phys. Lett. B* **789**, 1 (2019).
38. P.D.B. Collins. *An Introduction to Regge Theory and High-Energy Physics. Cambridge Monographs on Mathematical Physics* (Cambridge Univ. Press, 2009) [ISBN: 978-0-521-11035-8].
39. L.L. Jenkovszky, A.N. Wall. The dipole pomeron and structure in pp scattering. Preprint: ITF-74-166E (1974).
40. L.L. Jenkovszky, A.N. Wall. The dipole pomeron and pp scattering. *Czech. J. Phys. B* **26**, 447 (1976).
41. L.L. Jenkovszky. Phenomenology of elastic hadron diffraction. *Fortsch. Phys.* **34**, 791 (1986).
42. L.L. Jenkovszky, B.V. Struminsky, A.N. Shelkovenko. Odd C exchange in high-energy $\bar{p}p$ and pp scattering. *Z. Phys. C* **36**, 495 (1987).
43. P. Desgrolard, M. Giffon, L.L. Jenkovszky. Pomeron and odderon in high-energy pp and p anti-p elastic scattering. *Z. Phys. C* **55**, 637 (1992).
44. L.L. Jenkovszky, A.I. Lengyel, D.I. Lontkovskyi. The Pomeron and Odderon in elastic, inelastic and total cross sections at the LHC. *Int. J. Mod. Phys. A* **26**, 4755 (2011).
45. A.I. Lengyel, Z.Z. Tarics. Indirect evidence of the Odderon from the LHC data on elastic proton-proton scattering (2012). arxiv: 1206.5837 [hep-ph].
46. W. Broniowski, L. Jenkovszky, E. Ruiz Arriola, I. Szanyi. Hollowness in pp and $p\bar{p}$ scattering in a Regge model. *Phys. Rev. D* **98**, 074012 (2018).
47. I. Szanyi, N. Bence, L. Jenkovszky. New physics from TOTEM's recent measurements of elastic and total cross sections. *J. Phys. G* **46**, 055002 (2019).
48. I. Szanyi, L. Jenkovszky, R. Schicker, V. Svintozelskyi. Pomeron/glueball and odderon/oddball trajectories. *Nucl. Phys. A* **998**, 121728 (2020).
49. S. Donnachie, G. Dosch, P. Landshoff, O. Nachtmann. *Pomeron Physics and QCD* (Cambridge University Press, 2002) [ISBN: 978-0-511-53493-5].
50. A.I. Bugrij, G. Cohen-Tannoudji, L.L. Jenkovszky, N.A. Kobylinsky. Dual amplitudes with mandelstam analyticity. *Fortsch. Phys.* **21**, 427 (1973).
51. R. Fiore, L.L. Jenkovszky, F. Paccanoni, A. Prokudin. Baryonic regge trajectories with analyticity constraints. *Phys. Rev. D* **70**, 054003 (2004).
52. M.G. Albrow *et al.* Missing mass spectra in pp inelastic scattering at total energies of 23 GeV and 31 GeV. *Nucl. Phys. B* **72**, 376 (1974).

Received 21.11.25

I. Сані

СТРУКТУРА ПЕРЕРІЗІВ
ПРУЖНОГО ТА ОДИНАРНОГО
ДИФРАКЦІЙНОГО РОЗСІЯННЯ ПРОТОНІВ

Структура перерізів пружного протон-протонного розсіювання включає неекспоненційну поведінку в області малих $|t|$, а також дифракційний мінімум, за яким слідує максимум у $|t|$-розподілі. Обговорюється основна фізика такої структури та можливість появи подібної мінімально-максимальної картини в $|t|$-розподілі для однопротонного дифракційного розсіювання. Також представлена проста модель, що описує резонанси з малою масою в M^2-розподілі однодифракційного протон-протонного розсіювання.

Ключові слова: пружне протон-протонне розсіювання, дифракційне розсіювання, одинарна дифракційна дисоціація, резонанси, померон, одерон, "м'які" процеси.